ICAS 2016
30th Congress of the International Council of the Aeronautical Sciences
DCC, Daejeon, Korea ; September 25-30, 2016

DYNAMICS MODELLING FOR CONTROL OF AN UNSTEADY HYDRODYNAMIC STINGRAY ROBOT

Brittany Gater, Javid Bayandor
Virginia Tech

Keywords: *Bioinspiration, Computational Fluid Dynamics, Unsteady Hydrodynamics*

Abstract

To investigate the unsteady hydrodynamics of stingray locomotion, Computational Fluid Dynamics (CFD) determined pressure and shear force production for prescribed fin kinematics. A nonlinear equation for thrust production and steady swimming speed of the fin was developed through parametric analysis, which can be used for optimal velocity control in a batoid robot.

1 Introduction

Recently, technological advances in computers, mechatronics, and control methods have facilitated the development and plausibility of using robotic vehicles for exploration. As the field of ocean engineering develops new submersible vehicles to traverse and explore seas and oceans, the need for efficient propulsion and greater maneuverability for exploring and researching the undersea environment necessitates research into methods of transport other than propellers and jets. To address the need, researchers have turned to biological mechanisms for inspiration. Animals have had millions of years to develop optimal mechanisms for living in and navigating in their environments. For fish and aquatic mammals, their morphology allows them to specialize in either cruising, acceleration, or maneuverability [1]. Maneuverability is particularly challenging, and fishes skilled in difficult maneuvers tend to utilize undulation of long-based fins. A good example of this type of specialization and morphology is the superorder *Batoidea*, comprised of rays and skates. These creatures maneuver by using two large pectoral fins propagating undulating waves passing from the anterior to the posterior [2].

Although batoids typically move by passing a sinusoidal waveform along the length of their fin, the particular amplitude, frequency, and wave number vary depending on the species [2]. Analytical models have been developed to model the effect of these parameters on swimming dynamics, as in Lighthill's elongated body theory applied to balistiform and gymnotiform locomotion [3]. Additionally, studies of the vortical shedding resulting from fish swimming suggest an optimal range of frequency and amplitude for particular swimming speeds corresponding to a Strouhal number between 0.2 and 0.4 [4]. However, the particulars of undulatory locomotion, both in batoids and otherwise, are still under investigation. For example, the fin kinematics for the stingrays Taeniura lymma and Potamotrygon orbignyi, and how they relate to the overall swimming speeds, have been particularly investigated [5,6], lending some insight into the parameters used by these species. Of special note is the amplitude envelope found by Blevins and Lauder [6], which increased nearly linearly along the length of the middle section of the fin.

A very common approach to understanding undulatory dynamics is to design a robotic system approximating one or two fins, depending on the species used for inspiration. Generally, these fins

are mechanically discretized with a finite number of oscillating rods supporting transverse motion of the fin [7–14]. Visualization of the flow with particle image velocimetry (PIV) has been used to show the vortical shedding of the resulting von Karman wake structure [15, 16]. Another approach to investigating undulatory locomotion is to numerically solve the flow with computational fluid dynamics (CFD) for a continuous fin, usually with approximately constant amplitude along the length of the fin [17–21].

The previous study by Sharp et al [22] used CFD to investigate the effect of inlet speed on thrust production for a given set of kinematic parameters. The net thrust tended to vary nearly linearly with inlet velocity, with the thrust and drag balancing out around 0.76 m/s. Expanding on those results, Gater et al [23] discussed the results of an initial parametric study to determine the effect of each parameter on the resulting forces, moments, and power characteristics.

This study focuses on using two-dimensional (2D) computational fluid dynamics (CFD) and dimensional analysis to model the forward motion of a continuous robotic batoid fin for prescribed fin kinematics. As in [23], the amplitude envelope is approximated as linearly increasing along the entire length of the fin. Using results for the 2D case from that study, forces were separated into shear and pressure components and fit to equations quantitatively describing force production. The equations are used to determine steady swimming speed for a set of kinematics and the forces that would be present on a three-dimensional (3D) fin on a robotic system.

2 Methodology

2.1 Numerical Solver for CFD

The fluid dynamics for a dynamic 2D cross-section of a fin are solved using the commercial software ANSYS Fluent (v. 14.5). Assuming unsteady, incompressible flow, the continuity equation is:

$$\nabla \cdot \vec{v} = 0 \tag{1}$$

where $\vec{v}$ is the velocity vector. Neglecting gravitational effects, the incompressible unsteady momentum equation is:

$$\rho\left[\frac{\partial^2 \vec{v}}{\partial t^2} + \vec{v} \cdot (\nabla \vec{v})\right] = -\nabla p + \mu \nabla^2 \vec{v} \tag{2}$$

where ρ is the fluid density, t is time, p is the pressure, and μ is the dynamic viscosity.

The flow is solved using the segregated pressure-based Navier-Stokes (PBNS) with the semi-implicit method for pressure linked equations (SIMPLE) algorithm used to resolve pressure-velocity coupling. The gradients are discretized using the least squares cell based (LSCB) method. The momentum equations use second order implicit spatial discretization, while time is discretized using a first-order implicit method. The convergence criteria are set to 10^{-7} for continuity, x-velocity, and y-velocity. The appropriate size for the time step was estimated using the Courant-Fredrichs-Levy (CFL) number:

$$CFL = \frac{U\Delta t}{\Delta x} \tag{3}$$

where Δt is the time step and Δx is the smallest cell size. For all simulations, the CFL was less than one, with a maximum of 0.90. Additionally, the Reynolds number varied between 4×10^4 and 4×10^5 for all cases. Because the Reynolds number remained less than the critical Reynolds number and the solution converged for all cases, a laminar flow model was used.

An unstructured finite-volume mesh was generated around the cross-section and updated with each time step to retain simulation accuracy at all times, using a combination of diffusive smoothing and domain remeshing functions. At the start of each time step the diffusion function is

applied first, with the remeshing function occurring directly afterwards to correct for large mesh deformation.

The diffusive smoothing is modelled as:

$$\nabla \cdot (\gamma \nabla \vec{\psi}) = 0 \tag{4}$$

where the diffusion coefficient γ defines the degree to which the boundary motion $\vec{\psi}$ propagates through the surrounding fluid mesh. γ is calculated using the cell distance from the deforming boundary d.

$$\gamma = \frac{1}{d^a} \tag{5}$$

For this study, the diffusion parameter a was set to 1.75. Solving Eq. $\nabla \cdot (\gamma \nabla \vec{\psi}) = 0$(4) for $\vec{\psi}$, the mesh distribution at the next time step $\vec{x}_{t+1}$ is solved using ψ ¯, Δt and the present mesh distribution $\vec{x}_t$.

$$\vec{x}_{t+1} = \vec{x}_t + \vec{\psi}\Delta t \tag{6}$$

A remeshing function was then implemented to resolve the extreme boundary motions present in undulatory locomotion. A secondary mesh is used to retain the consistency of the fluid data during remeshing. The remeshing function uses the nodal distance from the nearest boundary d_{min} and the most remote node from the boundaries d_{max} to normalize the boundary distance (d_b):

$$d_b = d_{min}/d_{max} \tag{7}$$

d_b is then used to determine the cell size at the location of interest ($size_i$):

$$size_i = size_b \times \Gamma \tag{8}$$

where Γ is the sizing function factor, defined by the size function variation α and the size function rate β. Two different equations for Γ are implemented depending upon the sign of α:

$$\Gamma = 1 + a d_b^{1+2\beta}, \alpha > 0$$
$$\Gamma = 1 + a d_b^{\frac{1}{1-\beta}}, \alpha < 0 \tag{9}$$

Combining Eq. 8 and 9 yields the allowable size of a cell in the fluid volume. Using the remeshing functions with diffusion smoothing yields a robust, highly refined mesh as can be seen in Figure 1. The remeshing parameters used in this study were $\alpha = 1.1$ and $\beta = 0.15$. Figure 1 shows the unstructured 2D mesh immediately surrounding the fin cross-section at t=5s of simulation.

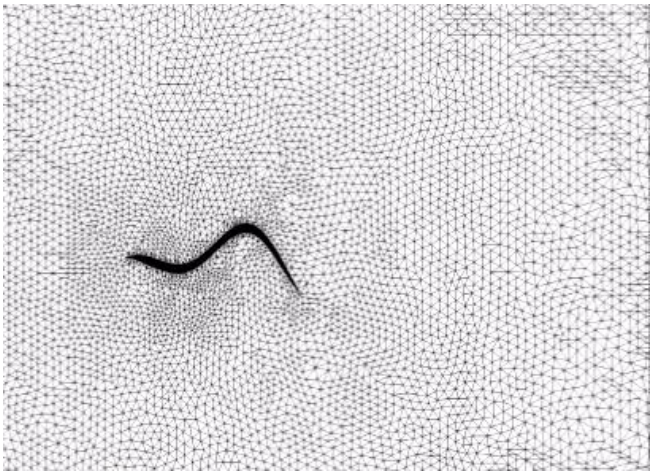

Figure 1: Mesh distribution around the undulating fin (black). Positive x and y are right and up, respectively.

Using the aforementioned computational methods, the forces acting on an element along the fin surface (F_i) are calculated using the pressure p and shear stress $\vec{\tau} = \mu \nabla^2 \vec{v}$:

$$\vec{F}_i = A(\nabla p + \nabla \cdot \vec{\tau}_i) \tag{10}$$

2.2 Computational Domain and Model

Because the fin length for the model was $L = 0.4$m, the domain used for CFD was 11.2×8m, with $7L$ in front of the fin and $20L$ behind the fin (with the x-direction oriented rearwards), and $10L$ above

and below the fin. Water uniformly enters the computational domain along the left boundary with a specified uniform velocity U. The upper and lower boundaries of the fluid domain are modelled with a symmetry condition and the right side set at ambient pressure $p = 0$.

The 2D fin was modelled using an approximation of the cross section of a batoid fin. To approximate the amplitude envelope for the kinematics determined by Blevins and Lauder [6], the centerline of motion is modeled as a sinusoid with linearly increasing amplitude propagating from front to rear of the fin, given by

$$y(x,t) = Ax \sin\left(2\pi\left(n\frac{x}{L} - ft\right)\right) \qquad (11)$$

and shown graphically in Figure 2. The fin motion variable y is the vertical displacement of the fin at distance x from the front, A is the slope of the amplitude envelope, n is the wave number (number of periods of the wave present on the fin), f is the frequency, x is a spatial coordinate whose origin is at the front of the fin and increases rightward, and t is time. Another useful parameter is wavelength $\lambda = L/n$, the length of one period on the fin. The fin is 0.4m in length, with a constant vertical thickness of 0.01m and linear tapering of the thickness in the anterior and posterior 0.05m.

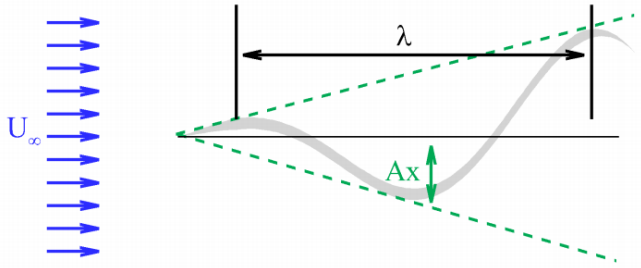

Figure 2: Swimming speed U of the fin model with wavelength λ, amplitude envelope Ax, and vertical flapping frequency f.

The cases run for the analysis were broken up into two parts: variations of U for a given set of kinematic parameters to determine the net zero F_x and parametric variation of kinematics for the U previously defined. The nominal case used was $U = 0.7625$m/s, $n = 1.19$, $f = 2.39$Hz, and $A = 0.25$. The parametric set consisted of variations of each parameter individually about this nominal case, as described in more detail in [23]. The fin frequency and wave number were chosen according to the range of the kinematics of the freshwater stingray *T. lymma* investigated by Rosenberger [5]. The slope of the amplitude envelope was based on the increasing amplitude region on the fin of the freshwater stingray *P. orbignyi* [6].

3 Method for Developing the Motion Model

The forces acting on the fin by the fluid result from two sources: pressure and shear. The total horizontal force was modeled as a combination of the two, and dimensional analysis was used to develop a generic model for the net force in terms of fluid and kinematic parameters. Using this generic model and data from the CFD trials, a numerical solver was employed to develop a best fit equation to describe the forces on the fin. Another parameter considered was the steady swimming speed, which we defined as the speed at which a given set of fin kinematics results in an average net zero horizontal force.

3.1 Shear Force

Because the Reynolds number is relatively large for the parametric study as a whole, the shear forces are small compared to the pressure forces. However, near the steady swimming speed, the total force is close to zero, meaning that shear plays a more significant role. In general, the steady swimming speed cannot be greater than the speed of the wave on the fin (wave speed). However, in the absence of viscous friction, these speeds should be identical, because from the law of conservation of momentum the wave speed on the fin forces the

fluid around it to move horizontally at the same speed. As such, shear forces can be used to predict the difference between the wave speed and steady swimming speed.

The equation model for shear force was based off of the dynamic viscosity as well as relevant velocity terms and length terms. The length terms considered were the length of the fin L, the wavelength $\lambda = L/n$, and the maximum fin amplitude AL. The velocity terms include the defined fluid speed U, the wave speed $f\lambda$, and the maximum vertical speed of a point on the fin $AL \cdot f$. To obtain the proper dimensions for force using these parameters, the form of the equation should be:

$$F_s/(width) = \mu(Velocity)(Length) \quad (12)$$

where the width refers to the dimension of the fin not captured by the 2D CFD model. The relevant length and velocity terms were then populated as follows:

$$Velocity = a_1 U + a_2 f\lambda + a_3 ALf \quad (13)$$

$$Length = b_1(A + b_2)L + b_3\lambda \quad (14)$$

where a_i, b_i are constants to be determined by solving for the best fit to the CFD data. Based on the results from the data, nondimensional terms such as A or n could also be included as needed. In particular, note that as the wave number n approaches zero, the shape of the fin in the flow approaches that of a flat plate. At that point, the force would not change with further changes in wavelength. To represent this scenario, the following nondimensional term was included in the analysis:

$$e\text{^}(-c_1/n) \quad (15)$$

where c_1 is positive to allow the term to approach zero as $1/n$ approached infinity.

After determining the constant terms providing the best fit for the data and model, the constants were evaluated to determine their relative importance to the overall force. If the constant resulted in a term that accounted for less than 0.1% of the total force for the range of parameter values, the term was removed, and the process was repeated. In this manner, only significant and relevant terms were included in the equations of best fit for the data.

3.2 Pressure Force

The magnitude of forces on the fin when not at steady swimming speed arise predominantly from pressure. Because steady swimming speed itself is determined by balancing the shear forces with the pressure forces, an understanding of both is necessary to develop an analytical model for controlling the speed of a robot. As such, the pressure forces are critical for developing both an initial open loop control of speed in a robot, and for developing a robust or optimal feedback controller for such a system.

Assuming these pressure forces can be modelled as dynamic pressure resulting from fluid density and velocity, dimensional analysis results in the following:

$$F_p/(width) = \tfrac{1}{2}\rho(Velocity)^2(Length) \quad (16)$$

The length term has the same form as for Eq. 14, although likely with different constants. For the velocity-squared V^2 term, the form used becomes:

$$V^2 = a_1 U^2 + a_2(f\lambda)^2 + a_3(ALf)^2 + a_4 U(f\lambda) + a_5 U(ALf) + a_6 f\lambda(ALf) \quad (17)$$

to account for different levels of interaction between the velocity variables. As before, the nondimensional terms, including Eq.15, can also be applied to the analysis to better represent the limits of the system.

3.3 Extension of the Model to a 3D Fin

Up to this point, the analysis has focused on developing a model for the 2D system. However, for a useful motion model, all three dimensions should be taken into account. Currently, the most common way to implement undulatory fins into a robotic design utilizes rods extending outward from the body which are actuated by servo motors. The rods are in turn connected by an elastic material that comprises the planform of the fin. The actuation mechanism, then, consists of radial motion from the base to the tip of the fin, and the position of a point on the fin is defined for an angle θ. For small angles, the fin motion can still be approximated by a vertical displacement y, as was used in the 2D analysis. The fin motion in three dimensional space would then be described as:

$$y(x,z,t) = A\left(\frac{z}{b}\right) x \sin\left(2\pi\left(n\frac{x}{L} - ft\right)\right) \quad (18)$$

where z is the distance along the span of the fin from base to tip, and b is the total width of that span. To model the 3D fin, we can model the individual cross sections of the fin and integrate along the span z. Assuming a rectangular fin with low amplitude, motion of the fluid directly influenced by the presence of effects in the z-direction will be small relative to the motion in the xy-plane modeled in CFD. Additionally, for forward motion, the frequency, wave number, and swimming speed is the same for all cross sections along the fin span; the only changing parameter is amplitude, which for a cross section at distance z from the body becomes $A\left(\frac{z}{b}\right)$. Then, integrating the resulting force (either shear or pressure) along the span yields the total force produced by that fin:

$$F_{fin} = \int_0^b \left(\frac{F}{width}\left(U, A\left(\frac{z}{b}\right), f, n\right)\right) dz \quad (19)$$

A robotic system also has mass m experiences drag from the body F_{body}, which is primarily a function of shape and velocity. These terms must also be incorporated into the model to determine the steady swimming speed and acceleration capabilities for the physical system. The motion model becomes a differential equation:

$$\frac{dv}{dt} = \frac{1}{m}\left(F_{fin}(U, A, f, n) + F_{body}(U)\right) \quad (20)$$

This motion model can then be used to develop more sophisticated controls for a robotic system.

4 Results

4.1 Parametric Study from CFD Model

Figures 3 and 4 show the shear and pressure force calculated from CFD, respectively, with respect to swimming speed and fin kinematics. Note that due to the orientation of the axes in the fin model, $F < 0$ corresponds to net forward force (net thrust) while $F > 0$ is net backward force (net drag).

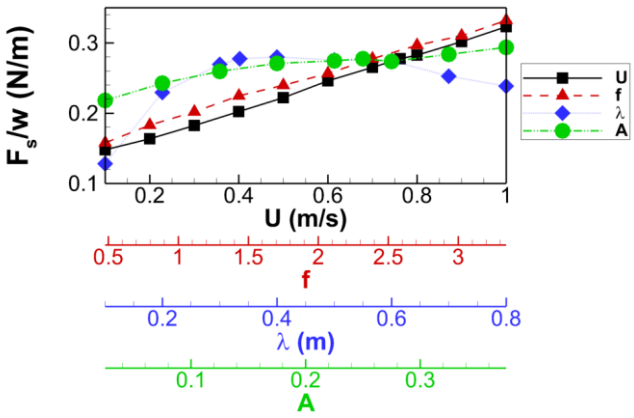

Figure 3: Net shear drag F_s as a function of swimming speed and fin kinematics.

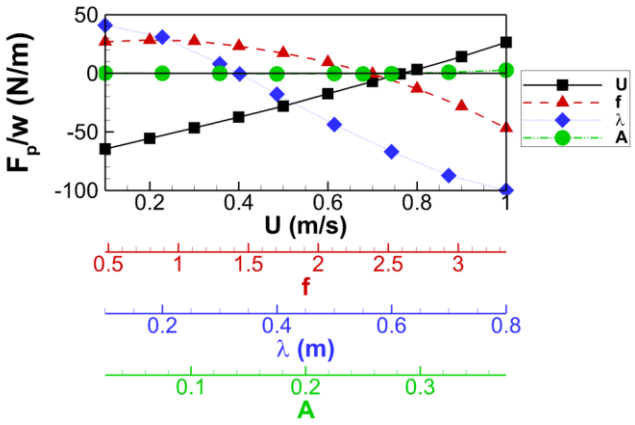

Figure 4: Net pressure drag F_p as a function of swimming speed and fin kinematics.

In general, the results from the figure correspond primarily to the pressure forces, with small contributions from shear. Note that each parameter has a single value at which F_p is zero, meaning that a particular set of fin kinematics must correspond to a single steady swimming speed. The following sections will discuss trends for the distinct pressure and shear forces more thoroughly.

4.2 Shear Force

With the first model for shear force, the resulting equation yielded a 99.875% fit with the given data. However, upon inspection of the fit for individual parameters and the resulting shear force, amplitude showed a relatively poor fit. For high amplitudes, the force was not well modelled. As such, a cubic term in nondimensional parameter A was incorporated to better represent the relationship from the data.

Using the new model for shear, one term was deemed negligible: $b_3\lambda$ in the length term. Removing $b_3\lambda$, the length term becomes $b_1(A + b_2)L$. Note, however, that A had already been modelled as a cubic function, providing an unnecessary level of redundancy. As such, $(A + b_2)$ was removed, and new constants were determined for the model.

Rearranging constants, the resulting model was:

$$F_s/w = 19618\mu\left(U + 1.87\frac{fL}{n} - 3.30ALf\right)L \cdot e^{-\frac{2.26L}{n}}(0.0234 + 0.153A - 0.425A^2 + A^3) \quad (21)$$

which had a 99.96% fit overall. Figure 5 shows the curves predicted by the model for F_s with the data to show the fit for amplitude.

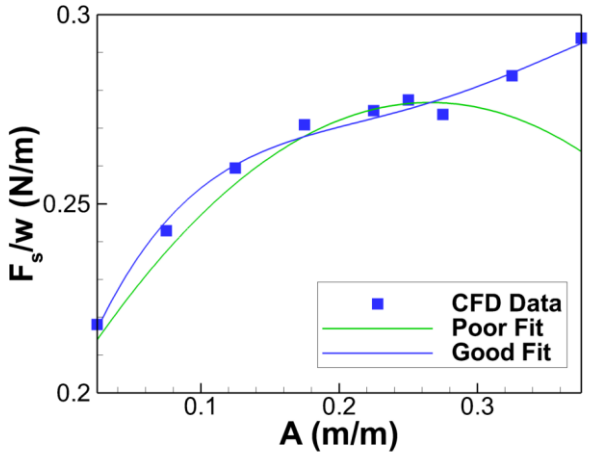

Figure 5: Shear force as a function of amplitude for model data for the poor fit and good fit equation.

4.3 Pressure Force

As with the shear force model, the initial pressure force model did not full represent all variable well. Although other parametric relationships fit well, the forces were not well modelled at low frequencies. The source of this poor fit was the term $(f\lambda)(ALf)$ in frequency from the V^2 term. When it was removed from the model, the resulting fit:

$$F_p/w = 0.675\rho((A - 0.0417)L - 0.0465\lambda) \cdot (U^2 - 3.75(f\lambda)^2 + 1.01(ALf)^2 + 2.99U(f\lambda) - 0.4148U(ALf)) \cdot e^{-\frac{0.502}{n}} \quad (22)$$

showed a much better correlation with the data, as shown in Figure 6.

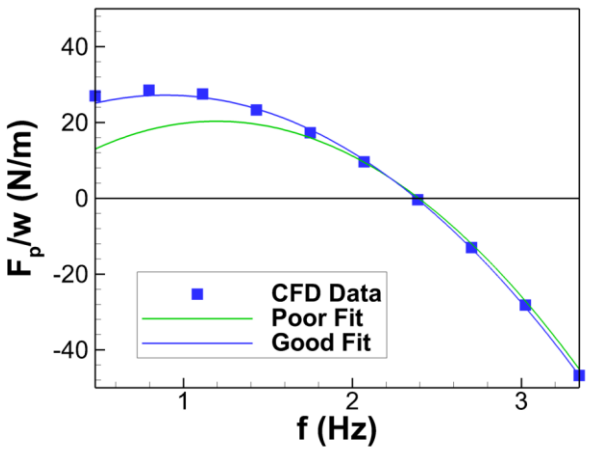

Figure 6: Pressure force as a function of frequency for model data for the poor fit and good fit equation.

4.4 3D Fin Forces

Once the forces along the span have been integrated, the result is approximately quadratic in U, cubic in A, quadratic in f, with more complex relationships for λ and n. Figure 7 shows the relationship between net drag (negative corresponds to thrust) and velocity for nominal fin kinematics and a fin width $b = 0.25$m. For brevity, the full equation is not shown here. However, in velocity, the modifications in going from 2D to 3D are simply a scalar change in F, with no change to the steady swimming speed.

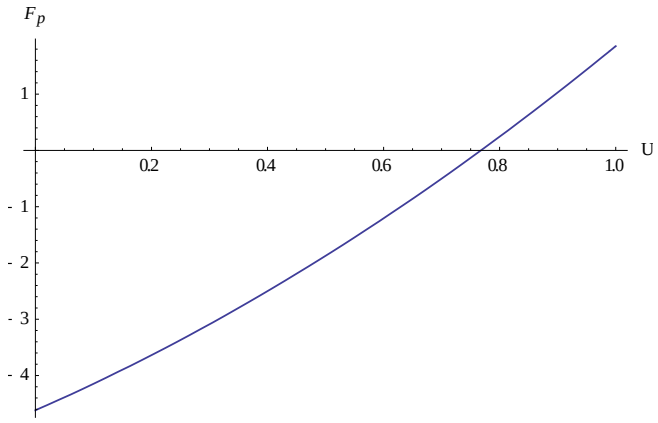

Figure 7: Pressure forces as a function of U for the 3D fin.

5 Discussion and Conclusions

Overall, the method of 2D CFD to determine trends for fin kinematics can be feasibly implemented with dimensional analysis for shear and pressure forces to determine the net drag or thrust on a 3D system. A set of fin kinematics can be used to determine the forward pressure force, and in turn the acceleration, on a body for a particular speed, yielding a first order ODE. These equations can then be linearized for optimal control, or used in its simple form to provide open loop control to a robotic system from an analytical model.

References

[1] P. W. Webb, “Form and Function in Fish Swimming,” *Sci. Am.*, vol. 251, no. 1, pp. 72–82, 1984.

[2] L. J. Rosenberger, “Pectoral fin locomotion in batoid fishes: undulation versus oscillation.,” *J. Exp. Biol.*, vol. 204, no. Pt 2, pp. 379–394, 2001.

[3] J. Lighthill and R. Blake, “Biofluiddynamics of balistiform and gymnotiform locomotion. Part 1. Biological background, and analysis by elongated-body theory,” *J. Fluid Mech.*, vol. 212, pp. 183–207, 1990.

[4] C. Eloy, “Optimal Strouhal number for swimming animals,” *J. Fluids Struct.*, vol. 30, no. 1, pp. 205–218, 2012.

[5] L. J. Rosenberger and M. Westneat, “Functional morphology of undulatory pectoral fin locomotion in the stingray taeniura lymma (Chondrichthyes:

dasyatidae),” *J. Exp. Biol.*, vol. 202 Pt 24, pp. 3523–39, 1999.
[6] E. Blevins and G. V. Lauder, “Rajiform locomotion: three-dimensional kinematics of the pectoral fin surface during swimming in the freshwater stingray Potamotrygon orbignyi,” *J. Exp. Biol.*, vol. 215, no. 18, pp. 3231–3241, 2012.
[7] O. M. Curet, N. A. Patankar, G. V. Lauder, and M. A. MacIver, “Mechanical properties of a bio-inspired robotic knifefish with an undulatory propulsor.,” *Bioinspir. Biomim.*, vol. 6, no. 2, p. 026004, 2011.
[8] K. H. Low, “Design, Development and Locomotion Control of Bio-Fish Robot With Undulating Anal Fins,” *Int. J. Robot. Autom.*, vol. 22, no. 1, 2007.
[9] J. Chen, T. Hu, L. Lin, H. Xie, and L. Shen, “Learning control for biomimetic undulating fins: An experimental study,” *J. Bionic Eng.*, vol. 7, pp. S191–S198, 2010.
[10] M. Jones and M. Joordens, “Design of an angular radial robotic stingray,” in *World Automation Congress (WAC)*, 2014, pp. 234–239.
[11] F. Liu, C. J. Yang, and K. M. Lee, “Hydrodynamic modeling of an undulating fin for robotic fish design,” *IEEE/ASME Int. Conf. Adv. Intell. Mechatronics, AIM*, vol. m, pp. 55–60, 2010.
[12] M. Sfakiotakis and J. Fasoulas, “Development and experimental validation of a model for the membrane restoring torques in undulatory fin mechanisms,” in *22nd Mediterranean Conference on Control and Automation (MED)*, 2014, pp. 1540–1546.
[13] Q. P. Wei, S. Wang, X. Dong, L. Shang, and M. Tan, “Design and kinetic analysis of a biomimetic underwater vehicle with two undulating long-fins,” *Acta Autom. Sin.*, vol. 39, no. 8, pp. 1330–1338, 2013.
[14] C. Zhou and K. H. Low, “Robust Tracking of Rhythmic Gait for a Biomimetic Robot,” *Int. J. Control Autom.*, vol. 7, no. 8, pp. 31–42, 2014.
[15] E. Blevins and G. V. Lauder, “Swimming near the substrate: a simple robotic model of stingray locomotion.,” *Bioinspir. Biomim.*, vol. 8, no. 1, 2013.
[16] R. P. Clark and A. J. Smits, “Thrust production and wake structure of a batoid-inspired oscillating fin,” *J. Fluid Mech.*, vol. 562, p. 415, 2006.
[17] M. M. Rahman, “Study on biomimetic squid-like underwater robots with two undulating side fins,” Osaka University, 2013.
[18] Y. Zhang, J. Laibin, J. H. He, J. Yang, S. Zhang, and K. H. Low, “A numerical analysis of an undulatory mechanical fin driven by Shape Memory Alloy,” *2006 IEEE Int. Conf. Robot. Biomimetics, ROBIO 2006*, vol. 4, pp. 73–78, 2006.
[19] W. Zhijun, C. Weishan, and S. Shengjun, “Influence of pectoral fin amplitude on batoid locomotion,” *Int. J. Adv. Inf. Sci. Serv. Sci.*, vol. 5, no. 7, pp. 129–137, 2013.
[20] A. A. Shirgaonkar, O. M. Curet, N. A. Patankar, and M. A. MacIver, “The hydrodynamics of ribbon-fin propulsion during impulsive motion.,” *J. Exp. Biol.*, vol. 211, no. 21, pp. 3490–3503, 2008.
[21] G. J. Dong and X. Y. Lu, “Numerical analysis on the propulsive performance and vortex shedding of fish-like travelling wavy plate,” *Int. J. Numer. Methods Fluids*, vol. 48, no. 12, pp. 1351–1373, 2005.
[22] N. Sharp, V. Hagen-gates, E. Hemingway, M. Syme, J. Via, J. Feaster, J. Bayandor, S. Jung, F. Battaglia, and A. Kurdila, “Computational Analysis of Undulatory Batoid Motion for Underwater Robotic Propulsion,” in *Proceedings of the ASME 2014 4th Joint US-European Fluids Engineering Division Summer Meeting*, 2014, pp. 1–8.
[23] B. Gater, J. Feaster, F. Battaglia, and J. Bayandor, “Dynamics and propulsive efficiency of bio-inspired undulatory marine locomotion,” in *ASME 2016 Fluids Engineering Division Summer Meeting*, 2016.

6 Contact Author Email Address

mailto:blgater@vt.edu

Copyright Statement